Intramolecular Vibrational Redistribution in the Vibrational Predissociation Dynamics of $He-I_2$

A. García-Vela[†]

Instituto de Matemáticas y Física Fundamental, CSIC, Serrano 123, 28006 Madrid, Spain

Received: March 17, 2006; In Final Form: May 10, 2006

The intramolecular vibrational redistribution (IVR) process is investigated in wave packet simulations of the vibrational predissociation dynamics of $He-I_2(B,v')$ in the region of high v' levels, $v' = 35-65$. The simulations indicate that for $v' \leq 45$ the dynamics is dominated by direct predissociation, whereas for higher v' levels the onset of IVR appears and becomes increasingly important. The IVR process occurs via coupling of the initial state in the v' manifold to intermediate long-lived resonances belonging to the lower $v < v'$ vibrational manifolds. The IVR dynamics manifests itself in multiexponential behavior and oscillations in the time-dependent population curves associated with the $He-I_2(B,v')$ initial state, the $He-I_2(B,v<v')$ intermediate complexes, and the final product states. The population curves corresponding to the $v' - 1$ intermediate resonances located below the $He + I_2(B,v'-1,j=0)$ dissociation limit are analyzed. It is found that initial population is transferred to all the intermediate resonance states considered, including those more separated in energy from the initial one. The results obtained for population transfer between the initial and the intermediate states can be explained by the intensity of the matrix elements coupling the initial and the intermediate resonances, in combination with the Rabi's formula for population exchange between two coupled states.

I. Introduction

At present, current lasers allow one a high degree of state-selectivity when polyatomic molecules are optically excited. However, this initial selectivity is typically lost as the dynamics evolves with time, due to intramolecular vibrational redistribution (IVR) processes. In principle, the occurrence of IVR is inherent to any molecular system, due to the fact that the initial state selectively excited is typically coupled to a manifold of vibrational states of the system, to which the initial state decays with time. Understanding the IVR process is a fundamental issue in chemical reaction dynamics, and the underlying IVR mechanisms have been extensively studied in a variety of systems. Some methods intended to prevent the occurrence of IVR have been proposed.[1−3]

Rare-gas−halogen van der Waals (vdW) complexes of the type Rg−BC are among the systems where IVR has been widely investigated, both theoretically and experimentally. Indeed, the IVR process has been studied in the framework of the vibrational predissociation (VP) of Rg−BC complexes, upon excitation of a vibrational level v' of BC within the B excited electronic state of the system. Several theoretical works investigating IVR in $Ar-Cl_2$,[4−6] $Ar-I_2$,[7] $He-Br_2$,[8,9] and $Ne-Br_2$,[10−12] have been reported. These works showed that IVR in the above Rg−BC-(B) complexes occurs through coupling of the initial state excited in the v' vibrational manifold to intermediate, doorway states correlating with the lower vibrational manifolds (mainly $v' - 1$). Other theoretical works have also found indications of IVR in the vibrational predissociation of $He-Br_2$ (ref 13) and $He-I_2$.[14] The signature of IVR has been observed experimentally in the VP of $Ar-Cl_2$,[15] $He-Br_2$,[9] and $Ne-Br_2$.[10] The observable manifestations of IVR were related to the rotational distributions of the diatomic fragment produced after VP through the $\Delta v' = -2$ vibrational dissociation channel. Such rotational distributions were found to be highly structured and highly dependent on the initial v' level excited.

Time-dependent pump−probe experiments on the VP of $Ne-Br_2(B,v'=16-29)$ have been carried out recently.[16] In these experiments it was found that for the higher v' excitations, the lifetimes estimated for appearance of Br_2 product fragments are significantly longer than the lifetimes corresponding to disappearance of the $Ne-Br_2(B,v')$ initial state. The delay between $Ne-Br_2$ disappearance and Br_2 product appearance might be related to temporary trapping of the $Ne-Br_2$ initial population in intermediate states before dissociation of the complex. Further wave packet calculations[17] on the $Ne-Br_2(B,v')$ VP confirmed this possibility. The calculations showed that for $v' > 22$ IVR becomes increasingly important, as a result of coupling between the initial state of $Ne-Br_2(B,v')$ and intermediate quasibound states corresponding to the lower $v < v'$ vibrational manifolds. The intermediate states are resonances embedded in the continuum of each $v < v'$ manifold, located above the $Ne + Br_2(B,v<v',j=0)$ dissociation limit, and resonances located below the $Ne + Br_2(B,v<v',j=0)$ dissociation limit. The IVR dynamics manifests itself in multiexponential behavior of the population curves corresponding to the $Ne-Br_2(B,v')$ disappearance and $Br_2(B,v<v')$ appearance, and in undulations displayed by these curves, originated by interference between the initial state, the intermediate quasibound states, and the product continuum states.

In a previous work,[14] indications of IVR dynamics were found in the VP of $He-I_2(B,v')$ for high v' levels. The $He-I_2(B,v')$ complex has been investigated in several experimental[18−22] as well as theoretical[23−25] works. However, to the best of the author's knowledge, the IVR in this system has not been studied in detail to date. This is the goal of the present paper, where wave packet simulations on the VP dynamics of $He-I_2(B,v')$

[†] E-mail: garciavela@imaff.cfmac.csic.es.

10.1021/jp061678p CCC: $33.50
Published on Web 06/13/2006

are reported for several v' excitations in the range $v' = 35-65$. In the current work, the evolving wave packet is projected out onto some of the intermediate quasibound states belonging to the $v' - 1$ vibrational manifold. More specifically, during the time evolution the wave packet is projected out onto the intermediate resonances located below the He + I_2(B,$v'-1$,j=0) dissociation limit. Such a projection allows one to monitor in time how the initial population flows toward the intermediate resonance states, making possible a more detailed analysis of the IVR mechanism.

The organization of the paper is the following. In section II the theoretical treatment used is described. In section III the results are presented and discussed. Conclusions are given in section IV.

II. Theoretical Treatment

The He−I_2 system is represented in Jacobi coordinates (r,R,θ), where r is the I−I bond length, R is the distance between He and the I_2 center-of-mass, and θ is the angle between the vectors **r** and **R** associated with the two radial coordinates. The potential-energy surface used for He−I_2(B) in the present calculations is an empirical fit reported in ref 14. All the calculations assumed total angular momentum $J = 0$.

The vibrational predissociation of He−I_2(B,v') has been simulated for six v' vibrational excitations, namely $v' = 35$, 45, 51, 57, 61, and 65. The initial state of the system is the ground resonance state of He−I_2(B,v'). In the previous Ne−Br_2(B,v') simulations,[17] the complex initial state was prepared in two different ways. In one case, the initial state consisted of the zero-order ground resonance state of Ne−Br_2(B,v'). In the other case, the ground vibrational state of the complex (corresponding to $v' = 0$) in the X electronic state was excited to the B state by means of a finite time width pulse, to resemble more closely the initial conditions of the time-dependent experiments of ref 16. This latter type of initial preparation creates in the B state a distribution of states around the resonance of interest, with a width inversely depending on the pulse time width. The subsequent dynamics was found to be similar for the two initial preparations of the system. In the current study it was chosen to start from the zero-order ground resonance of He−I_2(B,v') for the sake of simplicity in the analysis, because in this way the predissociation dynamics essentially corresponds to the resonance of interest.

Both the initial resonance state of the system and the intermediate quasibound states belonging to the $v' - 1$ vibrational manifold onto which the wave packet was projected out, were calculated variationally by expanding the resonance wave function as

$$\Phi(r,R,\theta) = \sum_{v,m,j} c^{(v)}_{m,j}\, \psi_m(R)\, \chi^{(j)}_v(r)\, P_j(\theta) \qquad (1)$$

In eq 1, $\chi^{(j)}_v(r)$ are the rovibrational eigenstates of I_2, $P_j(\theta)$ are normalized Legendre polynomials, and $\psi_m(R)$ are radial functions built up from a discrete variable representation (DVR) of sinc functions. In the basis set of eq 1, one vibrational state $v = v'$, and 25 Legendre polynomials (with even j) were used. Regarding the $\psi_m(R)$ functions, they are the so-called "wrapped" sinc functions,[26] which are defined as

$$\psi_m(R) = \phi_m(R) - \phi_m(-R), \qquad m = 1, ..., \infty \qquad (2)$$

where

$$\phi_m(R) = \Delta^{-1/2}\, \mathrm{sinc}\left[\pi\left(\frac{R}{\Delta} - m\right)\right] \qquad (3)$$

TABLE 1: Calculated He−I_2(B,$v'-1$) Resonance Energies Relative to the He + I_2(B,$v'-1$,j=0) Dissociation Limit

	$E_n^{(v'-1)}$ (cm^{-1})		
n	$v' - 1 = 50$	$v' - 1 = 60$	$v' - 1 = 64$
0	−13.193	−13.700	−14.336
1	−6.395	−6.154	−5.933
2	−5.008	−4.723	−4.461
3	−3.019	−3.282	−3.348
4	−0.837	−1.359	−1.747
5		−0.074	−0.138

[a] The index n is a collective index that labels the resonance states by their energy position.

with $\mathrm{sinc}(x) = \sin(x)/x$ and $\Delta = 0.25$ au the spacing between grid points. The above functions were used along with a quadrature where the grid points and weights are $R_m = m\Delta$ and $\omega_m = \Delta$, respectively. In the calculations 120 $\psi_m(R)$ functions were included in the basis set.

The ground resonance energies (corresponding to the initial states) for the $v' = 35$, 45, 51, 57, 61, and 65 levels are −13.56, −13.30, −13.19, −13.39, −13.83, and −14.53, respectively.[14] These energies are relative to the vibrational energy level of I_2(B,v',j'=0). The intermediate quasibound states below the He + I_2(B,$v'-1$,j=0) dissociation limit have been calculated for $v' - 1 = 50$, 60, and 64, and their energies are collected in Table 1. Five quasibound levels are found for the $v' - 1 = 50$ vibrational manifold, and six levels are obtained for the $v' - 1 = 60$, and 64 manifolds.

At this point, one might ask how justified it is to use a He−I_2(B,v') intermolecular potential that was fit to experimental information concerning the ground intermolecular level,[14] to calculate excited intermolecular states. One of the experimental quantities used to fit the potential surface was the predissociation lifetime. During the predissociation process, the system visits the continuum of the vibrational manifolds lower than v' ($v' - 1$, $v' - 2$, etc.), and therefore it samples the upper energy region of the intermolecular potential in those manifolds. Because the potential reproduces the lifetimes in good agreement with the experimental data, it indicates that the upper region of the intermolecular potential is realistic enough.

The vibrational predissociation dynamics is simulated by solving the time-dependent Schrödinger equation for the wave packet $\Phi(r,R,\theta,t)$, which is expanded as

$$\Phi(r,R,\theta,t) = \sum_{v,j} C_{v,j}(R,t)\, \chi^{(j)}_v(r)\, P_j(\theta)\, \mathrm{e}^{-\mathrm{i}E_v^{(j)}t/\hbar} \qquad (4)$$

where $E^{(j)}_v$ are the energy levels associated with the $\chi^{(j)}_v(r)$ states. The method to propagate the wave packet has been described in detail in ref 14. Only some of the parameters of the calculations have been modified in the present work, and they will be described next. The R coordinate is represented on a uniform grid consisting of 200 points with $R_0 = 0$ au and $\Delta R = 0.25$ au. The number of rotational states included in the expansion of eq 4 was 20 (with even j). The wave packet is absorbed in the limits of the R grid after each propagation time step, $\Delta t = 0.04$ ps, by multiplying each $C_{v,j}(R,t)$ packet by the function $\exp[-A(R - R_{abs})^2]$, for $R > R_{abs} = 43.0$ au, with $A = 0.5$ au^{-2}. It is considered that the vdW bond is effectively broken for distances $R > R_c = 20.0$ au. In all cases the wave packet propagation was carried out until a final time $t_f = 120$ ps.

III. Results and Discussion

A. Time-Dependent Population Curves and Lifetimes. The time evolution of the population curves for disappearance of

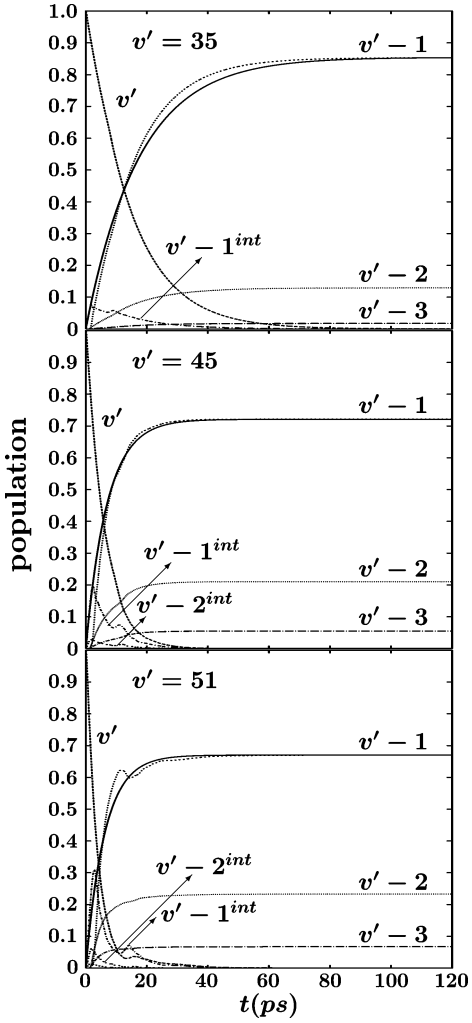

Figure 1. Population curves for disappearance of He−I_2(B,v'), appearance of I_2(B,v<v') products, and appearance of He−I_2(B,v<v') intermediate complexes (labeled as $v' - 1^{int}$, $v' - 2^{int}$) vs time, for $v' = 35$, 45, and 51. Exponential fits (solid lines) to the I_2(B,v'−1) appearance curves are also shown in the figure.

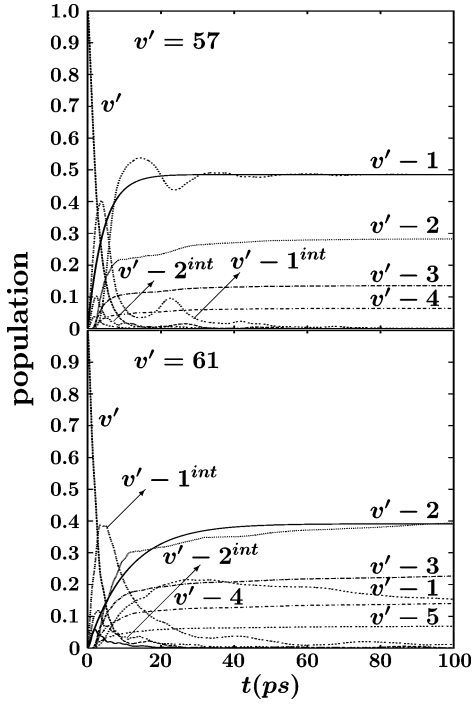

Figure 2. Same as Figure 1 but for $v' = 57$ and 61. Exponential fits (solid lines) to the I_2(B,v'−1) (for $v' = 57$) and I_2(B,v'−2) (for $v' = 61$) appearance curves are also shown in the figure.

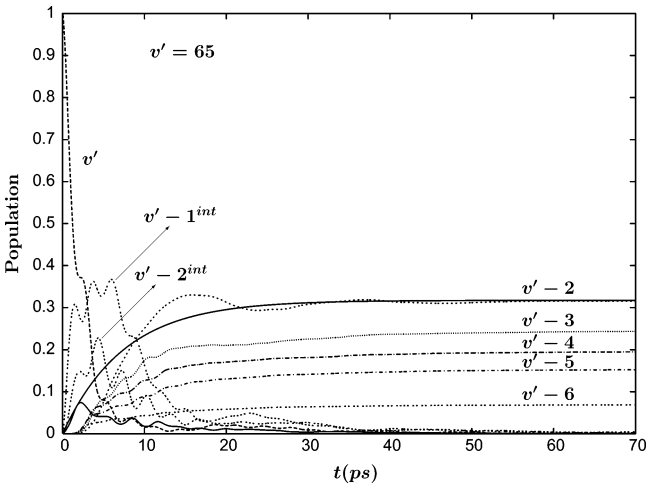

Figure 3. Same as Figure 1 but for $v' = 65$. An exponential fit (solid line) to the I_2(B,v'−2) appearance curve is also shown in the figure.

the He−I_2(B,v') initial state, for appearance of I_2(B,v<v') products (labeled as $v = v' - 1$, $v' - 2$, etc.), and for appearance of intermediate He−I_2(B,v<v') complexes (labeled as $v = v' - 1^{int}$, $v' - 2^{int}$) are shown in Figures 1−3 for the different v' levels studied. Due to the higher density of curves, the panels corresponding to $v' = 57$, 61, and 65 have been separated into two figures. Also, for the sake of clarity, in the abcissa of Figures 2 and 3 the time range has been reduced to 100 and 70 ps, respectively. The curves corresponding to the appearance of I_2(B,v<v') products and to the appearance of intermediate He−I_2(B,v<v') complexes were calculated by accumulating the wave packet probability in each dissociation channel in the regions $R > R_c = 20$ au and $R < R_c = 20$ au, respectively. In addition, Figures 1−3 show exponential fits, $P_v(t) \simeq A(1 - e^{-t/\tau})$ (being $A < 1$ an amplitude scaling coefficient[17]), to the population curves of the dominant dissociation channel, namely $v = v' - 1$ for $v' \leq 57$ and $v = v' - 2$ for $v' = 61$ and 65. This type of single-exponential fits were used to fit the experimental time-dependent appearance curves measured for the I_2 and Br_2 products obtained from predissociation of He−I_2(B,v')[22] and Ne−Br_2(B,v'),[16] respectively.

For $v' = 35$, the curves for the disappearance of He−I_2(B,v') and for the appearance of I_2(B,v<v') show an exponential behavior, indicating that the dynamics is dominated by direct predissociation of He−I_2(B,v') to the continuum, in a regime of a single, essentially isolated initial resonance. The case of $v' = 45$ is still similar, although the $v' - 1$ and $v' - 2$ I_2 appearance curves begin to display very slight undulations at short times, and the intermediate population curves $v = v' - 1^{int}$ and $v' - 2^{int}$ show bumps. For $v' \geq 51$, the undulations in the I_2(B,v<v') appearance curves become more intense, and a clear structure of bumps or recurrences appears in the curves corresponding to disappearance of He−I_2(B,v') and to appearance of intermediate He−I_2(B,v<v') complexes. This multiexponential behavior is a typical signature of IVR dynamics.[22,27] The maxima and minima appearing in the curves corresponding to the initial, intermediate, and fragment continuum states alternate, indicating exchange of population between all these states. The intensity of the population of intermediate complexes increases gradually with v'.

The undulations and recurrences displayed by the population curves of Figures 1−3, originating in multiexponential dynamics, were also found in the time-dependent curves calculated for VP of Ne−Br_2(B,v') in ref 17. Indeed, the state of the system initially prepared is close in energy and coupled to long-lived intermediate resonance states belonging to the lower $v < v'$ vibrational manifolds, in which the system population is temporarily trapped. The intermediate resonances can be located below the dissociation limit of the complex or can be embedded in the continuum of the corresponding $v < v'$ manifold. Intermolecular resonances embedded in the continuum above the dissociation limit have been spectroscopically accessed recently in the case of the He−ICl(B,v'=2) complex.[28] Interference and exchange of population along time between the v' initial resonance state, the $v < v'$ intermediate resonances, and the $v < v'$ product fragment continuum states is what causes the undulations in the corresponding population curves of Figures 1−3.

The increasing intensity of the population corresponding to the He−I_2(B,$v<v'$) intermediate complexes with increasing v' was also found in the Ne−Br_2(B,v') case.[17] This behavior was attributed in that work to an increasing density of the $v < v'$ intermediate resonances coupled to the initial state when v' increases. The underlying idea is that as the number of intermediate resonances coupled to the initial one increases, the probability of transfer of population from the initial state to the intermediate ones will increase correspondingly.

Actually, in the case of Ne−Br_2 the intensity of the $v' - 1$ intermediate population curve increased with v' up to $v' = 27$. For $v' \geq 28$, where the $\Delta v' = -1$ dissociation channel is already closed, the intensity of the $v' - 1$ intermediate population began to decrease. However, the intensity of the $v < v' - 1$ intermediate population curves increased monotonically with v' in all the range of v' levels studied.[17] The same behavior is displayed by the He−I_2 intermediate population curves of Figures 1−3. Indeed, the $v' - 1$ intermediate population curve increases in intensity with increasing v' up to $v' = 61$ and begins to decrease slightly for $v' > 61$, where the $\Delta v' = -1$ channel is energetically closed. The $v < v' - 1$ intermediate population curves, however, increase monotonically in intensity with increasing v'.

The above behavior was explained in the case of Ne−Br_2(B,v') by suggesting the following structure of the spectrum of intermediate resonances within each $v < v'$ vibrational manifold (Figure 10 of ref 17 shows a schematic view of such a spectrum). In this spectrum, the density of continuum resonance states would increase gradually as the energy decreases in the continuum region approaching the Ne + Br_2(B,$v<v'$,j=0) dissociation limit, reaching a maximum at energies around this limit. The density of the intermediate resonances turns to decrease as their energy keeps decreasing below the dissociation limit, as seen from the quasibound energy levels of Table 1.

Such a structure of the spectrum of intermediate resonances explains that the $v' - 1$ intermediate population, and therefore the IVR dynamics, reaches a maximum of intensity for a v' level near the closing of the $\Delta v' = -1$ dissociation channel. Indeed, as the initial v' level increases, the energy spacing between the v' and $v < v'$ vibrational manifolds decreases, and the initial ground resonance falls into a gradually denser and denser region of $v' - 1$ continuum resonances. For the highest v' level before the closing of the $\Delta v' = -1$ channel, the initial resonance is embedded in a region where the density of $v' - 1$ intermediate states is maximum, and coupling to these high number of states explains the maximum of the $v' - 1$ intermediate population. For higher v' levels (once the $\Delta v' = -1$ channel is closed), the initial resonance falls energetically below the $v' - 1$ dissociation limit, where the density of intermediate quasibound states coupled to the initial one turns to decrease, and therefore the intensity of the $v' - 1$ intermediate population curve decreases as well. The intensity of the $v < v' - 1$ intermediate populations increases monotonically with v' because the $\Delta v' < -1$ dissociation channels are still open, and the density of the $v < v' - 1$ intermediate continuum resonances coupled to the initial resonances is increasing monotonically with v'. Because the behavior of the population curves of the He−I_2(B,$v<v'$) intermediates is the same as that of the Ne−Br_2(B,$v<v'$) intermediates, it is expected that the spectrum of intermediate resonances suggested for Ne−Br_2 will also be valid for He−I_2.

TABLE 2: Calculated Lifetimes for Disappearance of He−I_2(B,v') and for Appearance of I_2(B,$v<v'$) Product Fragments. the Lifetimes for I_2 Appearance Correspond to I_2(B,$v'-1$) Products for $v' \leq 57$ and to I_2(B,$v'-2$) Products for $v' = 61$ and 65

	τ (ps)	
v'	disappearance of He−I_2	appearance of I_2 product
35	17.5	17.5
45	6.7	7.0
51	3.9	6.2
57	2.5	4.3
61	2.5	11.0
65	1.7	7.0

Related to the above discussion, it is interesting to note that the $v' - 1$ intermediate population curve that takes a longer time to decay is that corresponding to $v' = 61$, the highest level for which the $\Delta v' = -1$ dissociation channel is still open. Again, the same result was found for $v' = 27$ in Ne−Br_2(B,v').[17] This behavior is also related to the maximum of the density of long-lived intermediate resonances coupled to the initial state, reached for the highest v' level for which the $\Delta v' = -1$ channel is still open.

A remarkable feature in all of the intermediate population curves ($v' - 1^{int}$, $v' - 2^{int}$, $v' - 3^{int}$, etc.) in the $v' = 65$ case is the noticeable structure of peaks they display. Such a pronounced structure does not appear in the intermediate population curves calculated for the lower v' levels studied. This structure also was not found in the intermediate population curves calculated for Ne−Br_2(B,v'),[17] probably due to the fact that the highest v' level studied ($v' = 29$) was not sufficiently high. As we shall see below, the origin of this structure of peaks, at least in the case of the $v' - 1^{int}$ curve, is related to the probability transferred to the intermediate quasibound states located below the He + I_2(B,$v'-1$,j=0) dissociation limit.

So far the results show that the behavior of the different population curves obtained from the VP dynamics of He−I_2(B,v') is very similar to that found in Ne−Br_2(B,v'), indicating that the corresponding IVR mechanisms will be similar as well. It becomes now interesting to investigate what happens with the lifetimes associated with the disappearance of the He−I_2(B,v') initial state, and with the appearance of I_2(B,$v<v'$) product fragments, as was done experimentally[16] and theoretically[17] for Ne−Br_2. Lifetimes for He−I_2(B,v') disappearance were calculated in a previous work.[17] Lifetimes for I_2(B,$v<v'$) product appearance have been extracted in the current work by fitting the I_2(B,$v<v'$) appearance population curves corresponding to the dominant dissociation channel to an exponential function, as described in the beginning of this section. All the lifetimes are collected in Table 2.

It is found that the lifetimes for $He-I_2$ disappearance and for I_2 appearance are very similar for $v' = 35$ and 45. This result is expected from a direct predissociation dynamics. For $v' \geq 51$, the lifetimes for I_2 appearance become significantly longer than those associated with $He-I_2$ disappearance. Because this is the region of v' levels where IVR becomes important, it appears sensible to assign the delay between appearance of I_2 products and disappearance of $He-I_2$ to trapping of the initial population in long-lived intermediate resonances. Again, the same behavior was found for the corresponding lifetimes in $Ne-Br_2(B,v')$.[16,17] It is interesting to note the long I_2 appearance lifetime found for $v' = 61$, again the higher level just before the closing of the $\Delta v' = -1$ dissociation channel. Another similarity with the $Ne-Br_2$ case is the nonmonotonic behavior of the I_2 product appearance lifetimes with v'. Thus, the behavior of the time-dependent populations curves and lifetimes with v' in the VP of $He-I_2(B,v')$ is very similar to that found in $Ne-Br_2(B,v')$, which suggests similar IVR mechanisms.

B. Wave Packet Projection onto the $v' - 1$ Intermediate Resonances. The wave packet was projected out onto the $v' - 1$ intermediate quasibound states located below the $He + I_2(B,v'-1,j=0)$ dissociation limit. The projection was carried out onto the intermediate resonance states corresponding to $v' - 1 = 50$, 60, and 64, whose energy levels are collected in Table 1. Unfortunately, the intermediate resonances embedded in the continuum of the $v' - 1$ manifold (i.e., above the $He + I_2(B,v'-1,j=0)$ dissociation limit) cannot be converged through the bound state calculations described in section II, and therefore they were not included in the projection of the wave packet.

At this point, it is convenient to specify the energy position of the $He-I_2(B,v')$ initial state with respect to the energy location of the $v' - 1$ intermediate quasibound states. As mentioned in section II, the energies of the initial state of $He-I_2(B,v')$, relative to the I_2 vibrational energy level $E_{v'}^{(j'=0)}$, are -13.19, -13.83, and -14.53 cm^{-1} for $v' = 51$, 61, and 65, respectively. The I_2 vibrational spacings are $E_{v'}^{(j'=0)} - E_{v'-1}^{(j'=0)} = 29.90$, 14.60, and 9.92 cm^{-1} for $v' = 51$, 61, and 65, respectively. Thus, the energy level of the $He-I_2(B,v')$ initial state is located 16.71 cm^{-1} above, 0.77 cm^{-1} above, and 4.61 cm^{-1} below the $He + I_2(B,v'-1,j=0)$ dissociation limit for $v' - 1 = 50$, 60, and 64, respectively.

In Figure 4, population curves which accumulate the probability obtained by projecting out the wave packet onto all the $v' - 1$ intermediate quasibound states (labeled as $v' - 1^{sum}$), are shown vs time. For the sake of comparison, the population curves corresponding to the $He-I_2(B,v'-1)$ intermediate complexes are also presented in the figure. It should be noted that the difference in intensity between the $v' - 1^{sum}$ and the $v' - 1^{int}$ population curves is essentially due to the probability transferred to both the intermediate resonances embedded in the $v' - 1$ continuum and the $v' - 1$ continuum product fragment states (through direct predissociation). This probability is included in the $v' - 1^{int}$ curve but not in the $v' - 1^{sum}$ one.

For $v' = 51$, the intensity of the $v' - 1^{sum}$ curve is very small. This is not surprising because the initial state is energetically far from (and therefore weakly coupled to) the $v' - 1$ quasibound states onto which the wave packet is projected out. In the case of $v' = 51$, the initial state is expected to be more strongly coupled to continuum resonances in the $v' - 1$ manifold. As v' increases, the v' initial state becomes closer in energy, and therefore more strongly coupled to the $v' - 1$ intermediate quasibound states. As a result, the $v' - 1^{sum}$ population increases gradually, and for $v' = 65$ it accounts for most of the population of the $v' - 1^{int}$ curve.

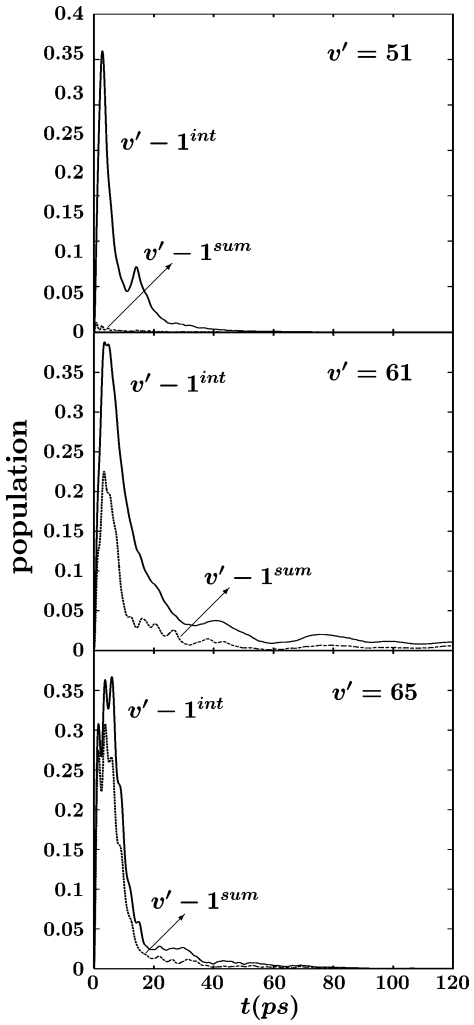

Figure 4. Population curves accumulating the probability transferred to all the $v' - 1$ intermediate resonance states of Table 1 (labeled as $v' - 1^{sum}$) vs time, for $v' = 51$, 61, and 65. The corresponding intermediate population curves, $v' - 1^{int}$, are also shown for comparison.

By comparing the $v' - 1^{sum}$ and $v' - 1^{int}$ curves corresponding to $v' = 61$ and 65, we find an intersting feature. At short times the two curves essentially coincide, but their intensities become increasingly separated as time proceeds. The implication is that, as long as the coupling bewteen the initial state and the $v' - 1$ intermediate quasibound states below the $He + I_2(B,v'-1,j=0)$ dissociation limit becomes sufficiently strong, this coupling acts in a shorter time scale than the coupling between the initial and the $v' - 1$ intermediate continuum resonances. We shall come back to this point later.

It is found, in the case of $v' = 65$, that both the $v' - 1^{int}$ and the $v' - 1^{sum}$ population curves present a similar structure of peaks at short times. Thus, as mentioned above, most of the structure of peaks of the $v' - 1^{int}$ curve is due to initial wave packet intensity transferred to the intermediate quasibound states below the $v' - 1$ dissociation limit, rather than to $v' - 1$ intermediate continuum resonances. This structure will be analyzed in more detail below.

The $v' - 1^{sum}$ population curves, which accumulate the probability transferred to all of the quasibound states considered in the wave packet projection, are not observable. However, the time-dependent population curves corresponding to each $v' - 1$ intermediate quasibound state can be, in principle, observed experimentally. These curves are shown in Figures 5 and 6 for

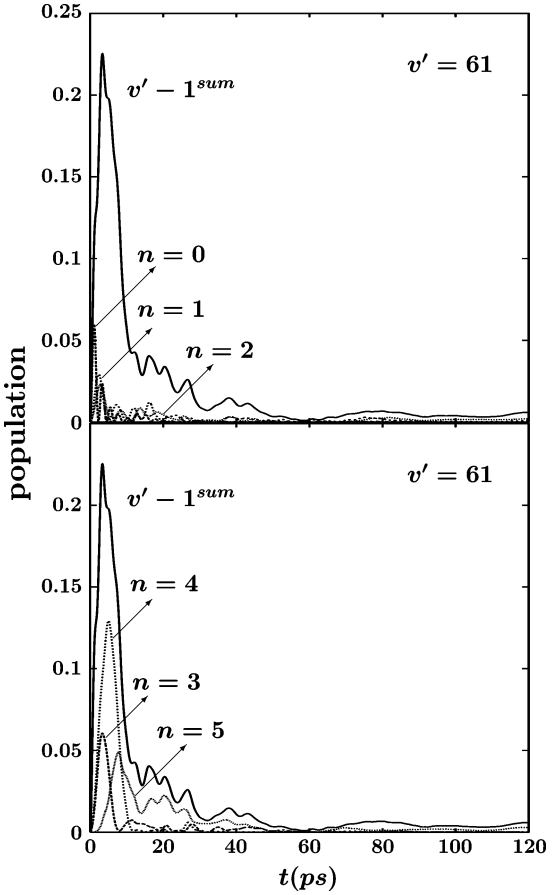

Figure 5. Population curves corresponding to each $v' - 1$ intermediate resonance state (labeled by the n index) vs time for $v' = 61$. The corresponding $v' - 1^{sum}$ population curve is also shown for comparison.

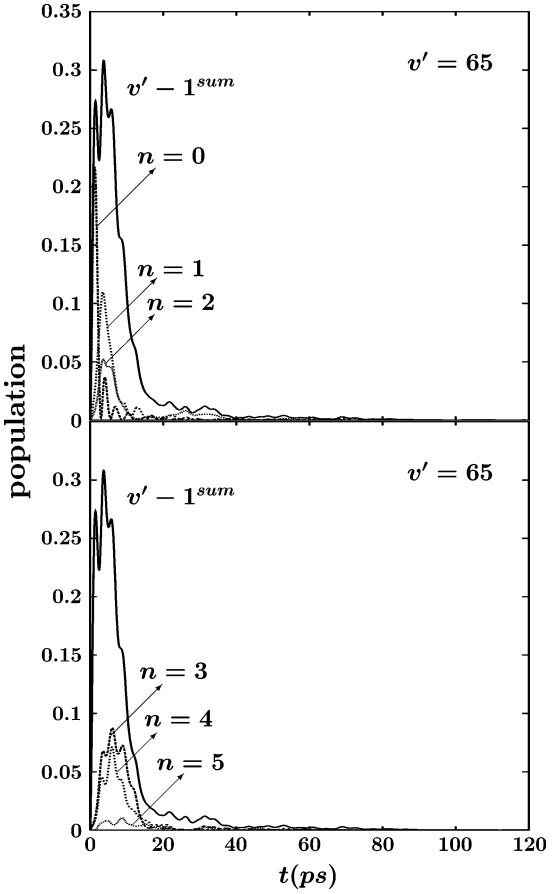

Figure 6. Same as Figure 5 but for $v' = 65$.

$v' = 61$ and 65, respectively, along with the corresponding $v' - 1^{sum}$ curves for the sake of comparison.

Interestingly, the curves of Figures 5 and 6 show that the initial state is appreciably coupled to all the $v' - 1$ quasibound states considered, and not only to those closer in energy. Indeed, a substantial amount of initial probability goes to the $n = 0$ quasibound state at short times, for both $v' = 61$ and 65, despite that this state is separated from the initial one by $\sim$14 cm^{-1} and $\sim$10 cm^{-1}, respectively. In the previous work[17] on Ne−Br_2(B,v') it was assumed that the coupling of the initial state was effective essentially with nearly degenerate intermediate resonances of the lower vibrational manifolds. The present result appears to indicate that the initial state is effectively coupled to intermediate states located in a relatively large range of energy. This situation seems to be different to that found for Ar−Cl_2(B,v'>8),[5] where the IVR mechanism proceeds via coupling to mainly one $v' - 1$ intermediate quasibound state rather close in energy to the initial resonance state.

Another interesting feature is that the $v' - 1$ quasibound states that reach the maximum of population are not the closest ones in energy to the v' initial state. For $v' = 61$ and 65, the quasibound states closest in energy to the initial state are $n = 5$ and $n = 2$, respectively. However, the maximum intensity of population is reached for $n = 4$ and $n = 0$ in the cases of $v' = 61$ and 65, respectively. A possible explanation is that the matrix elements coupling the initial and these intermediate states are larger. Indeed, the coupling matrix elements between the initial and the intermediate states are expected to be larger as the quantum numbers in the intermolecular modes of the initial state ($n = 0$) become more similar to those of the quasibound intermediate states (i.e., low n).

The matrix elements between the initial and the intermediate quasibound states have been calculated for $v' = 61$ and 65. For $v' = 61$, these matrix elements are 1.02×10^{-5}, 3.51×10^{-6}, 2.48×10^{-6}, -3.29×10^{-6}, 3.82×10^{-6}, and 2.12×10^{-7} au, for $n = 0-5$, respectively. The matrix elements for the $v' = 65$ initial state are -1.71×10^{-5}, 4.67×10^{-6}, -2.85×10^{-6}, -3.32×10^{-6}, -3.41×10^{-6}, and 1.01×10^{-6} au, for $n = 0-5$, respectively. For the two v' levels, the largest matrix element is that corresponding to the lowest $n = 0$ intermediate quasibound state. However, for $v' = 61$ the second largest matrix element corresponds to the $n = 4$ quasibound state, whereas the $n = 5$ matrix element is the smallest one. For $v' = 65$, the $n = 0$ matrix element is comparatively larger than in the $v' = 61$ case, and the $n = 2$ matrix element is the second smallest one. Thus, there appears to be a relation (at least partial) between the magnitude of the matrix elements coupling the initial and the intermediate quasibound states and which quasibound state reaches the maximum population.

The results show that the lowest quasibound states ($n = 0$, 1) are the first ones being populated, for both $v' = 61$ and 65. Actually, the curves of Figures 5 and 6 show that the order in which the intermediate quasibound states begin to be populated along time, follows the order of their energy position, namely, first $n = 0$, then $n = 1$, then $n = 2$, etc. In general, the population curves associated with the $v' - 1$ quasibound states display a structure of peaks, in the cases of both $v' = 61$ and 65. This structure is more pronounced in the curves of the $v' - 1 = 64$ quasibound states, and the superposition of all the individual structures give rise to the structure of peaks displayed by the $v' - 1^{sum}$ population curve. The structure of peaks in the population

curve of each intermediate state indicates that the population is transferred or exchanged by "beats".[27] In addition, the peaks in each curve are typically separated by a rather constant amount of time, and the curves associated with the lower quasibound states (more separated in energy from the initial one) present a higher number of oscillations.

The behavior and the structure of the population curves of Figures 5 and 6 can be explained by the Rabi's formula[29] for the exchange of probability between two coupled states. According to this formula, the time-dependent behavior of the probability transferred from the initial to a given intermediate state is given by $P_{if}(t) = [4|W_{if}|^2/(4|W_{if}|^2 + (E_i - E_f)^2)] \sin^2[(4|W_{if}|^2 + (E_i - E_f)^2)^{1/2}t/2\hbar]$, where E_i and E_f are the energies of the initial and intermediate states, respectively, and W_{if} is the coupling between them. This formula shows that as the $E_i - E_f$ energy separation increases, the population exchange oscillates faster in time, as found in Figures 5 and 6.

Figures 5 and 6 show that the population curves of some of the intermediate states extend up to 40 ps with appreciable intensity. Some curves extend for longer times, reaching up to 100 and 120 ps, albeit with a substantially lower intensity. However, a period of 40 ps might be long enough to detect experimentally some of the population curves.

IV. Summary and Conclusions

Wave packet simulations of the vibrational predissociation of He−I_2(B,v') were carried out for high vibrational levels v' ($v' = 35$, 45, 51, 57, 61, and 65) to investigate the IVR dynamics in this system. Time-dependent population curves for disappearance of the He−I_2(B,v') initial state and for appearance of He−I_2(B,$v<v'$) intermediate complexes and I_2(B,$v<v'$) product fragments were computed. For $v' = 35$ and 45, the population curves show a single exponential behavior, consistent with a dynamics essentially dominated by direct predissociation. For $v' \geq 51$, IVR dynamics manifests itself in the form of multiexponential behavior and oscillations in the different population curves. The IVR process occurs via coupling of the system initial state to $v < v'$ intermediate long-lived resonances located both in the continuum and below the dissociation limit of the $v < v'$ vibrational manifolds. The oscillations found in the population curves indicate that the v' initial state, the $v < v'$ intermediate resonance states, and the $v < v'$ product continuum states are coupled, and they interfere and exchange population along time. It is also found that the population of the He−I_2(B,$v<v'$) intermediate complexes increases gradually with v', reflecting that the probability of IVR dynamics is enhanced with increasing v'.

Lifetimes for disappearance of the He−I_2(B,v') initial state and for appearance of I_2(B,$v<v'$) products were computed. For $v' = 35$ and 45, the lifetimes obtained for He−I_2(B,v') disappearance and I_2(B,$v<v'$) appearance were very similar, confirming that in this region of v' levels the dynamics is dominated by direct predissociation. For $v' \geq 51$, the I_2(B,$v<v'$) appearance lifetimes become significantly longer than those for He−I_2(B,v') disappearance, suggesting that the initial population is temporarily trapped in intermediate long-lived resonances.

Time-dependent population curves corresponding to some of the $v' - 1$ intermediate resonance states, specifically those located below the He + I_2(B,$v'-1$,j=0) dissociation limit, have been computed by projecting out the wave packet onto such states. This allowed for a more detailed analysis of the IVR mechanisms. It is found that the initial population is transferred to all the intermediate resonances considered, not only those closer in energy to the initial state. In fact, the maximum transfer of population occurs for intermediate resonances which are not the closest ones in energy to the initial state. The initial population is transferred to the lower intermediate resonances (more separated in energy from the initial state) in a shorter time scale, and this time scale increases with increasing energy of the intermediate resonances. In addition, the population curves of individual intermediate resonances display a structure of peaks, separated by a rather constant period of time. All these results can be rationalized in terms of the intensity of the matrix elements coupling the initial and the intermediate resonances, combined with the Rabi's formula for the exchange of population between two coupled states. This formula predicts an oscillating behavior in time of the population exchange, depending on the coupling and the energy separation between the initial and a given intermediate state.

Finally, the IVR behavior found in this work for He−I_2(B,v'), regarding the population curves of the initial, intermediate, and final product states, as well as the lifetimes for He−I_2(B,v') disappearance and I_2(B,$v<v'$) product appearance, is very similar to that previously obtained for Ne−Br_2(B,v').[17] Thus, these results come to support the hypothesis that the IVR mechanism suggested is general to a variety of rare-gas−halogen vdW complexes.

Acknowledgment. This work was funded by CICYT (Ministerio de Educación y Ciencia), Spain, Grant No. FIS-2004-02461. The Centro de Supercomputación de Galicia (CESGA) and the Grupo de SuperComputación del CIEMAT (GSC) are acknowledged for allocation of computer time.

References and Notes

(1) Mukamel, S.; Shan, K. *Chem. Phys. Lett.* **1985**, *117*, 489.
(2) Sleva, E. T.; Glasbeek, M.; Zewail, A. H. *J. Chem. Phys.* **1986**, *90*, 1232.
(3) Vreeker, P.; Glasbeek, M.; Sleva, E. T.; Zewail, A. H. *Chem. Phys. Lett.* **1986**, *129*, 117.
(4) Halberstadt, N.; Beswick, J. A.; Roncero, O.; Janda, K. C. *J. Chem. Phys.* **1992**, *96*, 2404.
(5) Halberstadt, N.; Serna, S.; Roncero, O.; Janda, K. C. *J. Chem. Phys.* **1992**, *97*, 341.
(6) Roncero, O.; Villarreal, P.; Delgado-Barrio, G.; Halberstadt, N.; Janda, K. C. *J. Chem. Phys.* **1993**, *99*, 1035.
(7) Gray, S. K. *Chem. Phys. Lett.* **1992**, *197*, 86.
(8) González-Lezana, T.; Hernández, M. I.; Delgado-Barrio, G.; Villarreal, P. *J. Chem. Phys.* **1997**, *106*, 3216.
(9) Rohrbacher, A.; Ruchti, T.; Janda, K. C.; Buchachenko, A. A.; Hernández, M. I.; González-Lezana, T.; Villarreal, P.; Delgado-Barrio, G. *J. Chem. Phys.* **1999**, *110*, 256.
(10) Nejad-Sattari, M.; Stephenson, T. A. *J. Chem. Phys.* **1997**, *106*, 5454.
(11) Stephenson, T. A.; Halberstadt, N. *J. Chem. Phys.* **2000**, *112*, 2265.
(12) Miguel, B.; Bastida, A.; Zúñiga, J,; Requena, A.; Halberstadt, N. *J. Chem. Phys.* **2000**, *113*, 10130.
(13) García-Vela, A. *J. Phys. Chem. A* **2005**, *109*, 5545.
(14) García-Vela, A. *J. Chem. Phys.* **2005**, *123*, 124311.
(15) Evard, D. D.; Bieler, C. R.; Cline, J. I.; Sivakumar, N.; Janda, K. C. *J. Chem. Phys.* **1988**, *89*, 2829.
(16) Cabrera, J. A.; Bieler, C. R.; Olbricht, B. C.; van der Veer, W. E.; Janda, K. C. *J. Chem. Phys.* **2005**, *123*, 054311.
(17) García-Vela, A.; Janda, K. C. *J. Chem. Phys.* **2006**, *124*, 034305.
(18) Johnson, K. E.; Wharton, L.; Levy, D. H. *J. Chem. Phys.* **1978**, *69*, 2719.
(19) Kenny, J. E.; Johnson, K. E.; Sharfin, W.; Levy, D. H. *J. Chem. Phys.* **1980**, *72*, 1109.
(20) Blazy, J. A.; Dekoven, B. M.; Russell, T. D.; Levy, D. H. *J. Chem. Phys.* **1980**, *72*, 2439.
(21) Sharfin, W.; Kroger, P.; Wallace, S. C. *Chem. Phys. Lett.* **1982**, *85*, 81.
(22) Gutmann, M.; Willberg, D. M.; Zewail, A. H. *J. Chem. Phys.* **1992**, *97*, 8037.
(23) Beswick, J. A.; Delgado-Barrio, G. *J. Chem. Phys.* **1980**, *73*, 3653.
(24) Gray, S. K. *Faraday Discuss.* **1994**, *97*, 143.

(25) Seong, J.; Sun, H.; Ratner, M. A.; Schatz, G. C.; Gerber, R. B. *J. Phys. Chem.* A **1998**, *102*, 9345.
(26) Groenenboom, G. C.; Colbert, D. T. *J. Chem. Phys.* **1993**, *99*, 9681.
(27) Felker, P. M.; Zewail, A. H. *Adv. Chem. Phys.* **1988**, *70*, 265.
(28) Darr, J. P.; Loomis, R. A.; McCoy, A. B. *J. Chem. Phys.* **2005**, *122*, 044318.
(29) See for example: Cohen-Tannoudji, C.; Diu, B.; Laloë, F. *Quantum Mechanics*; Hermann: Paris, 1977; Vol. I, p 441.